

ICSO 2016

International Conference on Space Optics

Biarritz, France

18–21 October 2016

Edited by Bruno Cugny, Nikos Karafolas and Zoran Sodnik



Correlation of Ingenio/Seosat radiometric model with the results of the radiometric campaigns

C. Miravet

D. Zorita

C. Santos

J. Sanchez

et al.



icso proceedings



CORRELATION OF INGENIO/SEOSAT RADIOMETRIC MODEL WITH THE RESULTS OF THE RADIOMETRIC CAMPAIGNS

C. Miravet¹, D. Zorita¹, C. Santos¹, J. Sánchez¹, G. Taubmann¹, A. Rodríguez Alija², I. Cabeza³, A. Marini⁴

¹SENER Ingeniería y Sistemas, c\Severo Ochoa 4, PTM, Tres Cantos, 28760 Madrid, Spain.

²THALES-ALENIA Space, c\Einstein 7, PTM, Tres Cantos, 28760 Madrid, Spain.

³AIRBUS Defence and Space, Avda. de Aragón 404, 28022 Madrid, Spain.

⁴ESTEC-ESA, postbus 299, Keplerlaan 1, 2200 AG Noordwijk, The Netherlands.

INTRODUCTION

Ingenio/SEOSAT is a multi-spectral high-resolution optical satellite for Earth remote sensing, designed to provide imagery to different Spanish civil, institutional and governmental users, and potentially to other European users in the frame of GMES and GEOSS. In this communication, it is presented the Ingenio/SEOSAT radiometric signal model and specifically its correlation with the results of radiometric campaigns performed at subsystem (focal plane) and system (complete camera) levels.

Ingenio/SEOSAT flight radiometric signal model encompasses the combined contribution of all elements of the acquisition chain, from input top-of-atmosphere (TOA) radiance to digital output. The conversion from radiance to digital output could be thought of conceptually as a sequential process involving three different steps. In the first step, input radiance is focalized by the telescope optics onto the detector surface, providing an image with an associated irradiance. Then, this irradiance generates a number of photo-electrons in the CCD detector. In the third step, this signal is first transformed to voltage at the detector output, and finally is amplified and converted to a digital signal by the proximity and video unit electronics, respectively.

To perform an accurate model correlation with the measurements, specific signal models at focal plane and complete camera levels have been generated. These models have been derived from SEOSAT flight signal model, after adaptation to reproduce the specific conditions of the performed radiometric tests, in matters such as the spectral characteristics of the used illumination sources, or the actual definitions of mean radiance and irradiance considered in the tests.

These signal models have been used to compute the following data, on a pixel-by-pixel basis: (a) signal transfer functions relating input radiance to digital output, as measured at camera level; (b) signal transfer functions relating input irradiance to digital output, as measured at focal plane level;

Away from the saturation region, these signal transfer functions can be considered as linear with very good approximation. For measurements at focal plane level, the function slopes contain the combined contribution of steps two and three described above, encompassing the conversion from focal plane irradiance to digital signal. The contribution of each of these steps could be further discriminated through the use of photon transfer curves, as briefly described in a dedicated section. Finally, signal transfer function slopes at camera level contain also the contribution of optics. In fact, the ratio of slopes at camera and focal plane levels is a quantity that depends only on telescope parameters, being related to the conversion of input radiance to focal plane irradiance.

The slopes of the transfer functions predicted by the radiometric models have been compared to the experimental results at both camera and focal plane levels. From these comparisons, correction factors needed for the models to reproduce the actual radiometric behavior of telescope and focal planes have been derived. Finally, these alignment factors between model predictions and measurements have been used together with the flight signal model in the derivation of flight saturation level predictions, a topic not covered in this communication.

This communication presents in detail the methodology and results of the performed correlation study. The devised procedure provides a method to derive camera correction factors from telescope and focal plane contributors. This is especially convenient at project stages where complete camera radiometric measurements are only available for engineering qualification models, whereas radiometric measurements for flight focal plane units have already been performed. Also, it constitutes a system-level approach to determine the contribution to the output signal of different blocks of the acquisition chain, based exclusively on results generally available from different radiometric campaigns.

SEOSAT PRIMARY PAYLOAD

Ingenio/SEOSAT [1-4] is a multi-spectral high-resolution optical satellite for Earth remote sensing, designed to provide imagery to different Spanish civil, institutional and governmental users, and potentially to other European users in the frame of GMES and GEOSS. Ingenio/SEOSAT is a Low Earth Orbiting mission. It features a Primary Payload (PP) with one 2.5 meter resolution panchromatic channel and four 10 meter resolution visible/near infrared spectral channels. The PP swath close to 55 km ensures a frequent revisit period, and offers quick accessibility to any point on Earth in emergency situations.

A 3D view of the payload is presented in fig. 1. The payload is equipped with two identical cameras, each covering half of the requested image swath. Following the light path, each camera is composed of the following elements:

- An optical telescope based on an all-reflective Korsch concept.
- A focal plane assembly composed of two panchromatic (PAN) plus two multi-spectral (MS) detectors, co-planarly located. Detectors for both channels are of CCD type. The detectors used for the PAN channel are based on Time Delay and Integration (TDI) technology to increase the number of generated photo-electrons, with the corresponding improvement in signal-to-noise ratio. A 4-line CCD detector has been used for the MS channel, with lines devoted to sense blue, green, red and NIR spectral bands. Both PAN and MS detectors are mounted on its proper sub-assembly, which includes the filters defining the spectral bands and the corresponding proximity electronics.
- The electronics modules, including the electronic video units, the video power supply and the interface and control electronics.



Fig. 1. 3D view of the Ingenio/SEOSAT primary payload

FOCAL PLANE RADIOMETRIC SIGNAL MODEL

In this section is described the used theoretical signal model at focal plane level, based on the information supplied by the manufacturers of the different components. Focal plane (FP) is understood here as the sub-system consisting of: a) spectral filters; b) detectors; c) proximity electronics; d) video unit (VU) electronics.

Complete radiometric campaigns have been performed by TAS-E on this subsystem, for the engineering-qualification model (EQM) and the two flight models (FM+, FM-). In fig. 2 is presented a diagram of the set-up used for the radiometric campaigns at FP level. An integrating sphere with an aperture of 1" is placed perfectly aligned to the center of the focal plane, at a distance of 270 mm. This configuration reproduces the size and location of the exit pupil in the camera.

The irradiance at the FP could be varied by means of a motorized diaphragm located at the illumination port of the integrating sphere. This enables setting different radiometric scenarios covering the dynamic range of both the PAN and MS bands. For each scenario, corresponding to a given setting in the diaphragm aperture, the

irradiance at the center of the FP has been measured, replacing the FP by a spectro-radiometer located at its center. The irradiance distribution provided by the integrating sphere at several locations in the focal plane was also measured with the spectro-radiometer, founding an excellent agreement with the expected \cos^4 law.

Hence, a large number of digital image data in the different spectral bands, associated to different levels of irradiance in the FP center, are available as a result of a FP radiometric campaign. This data has been used to generate experimental plots of digital signal vs. FP center irradiance for each pixel in the PAN and the four MS spectral bands. These plots are almost perfectly linear, away from the detector saturation region. The slopes of these plots have been compared to the ones predicted by the signal model, to derive correction factors to align signal model predictions to experimental results.

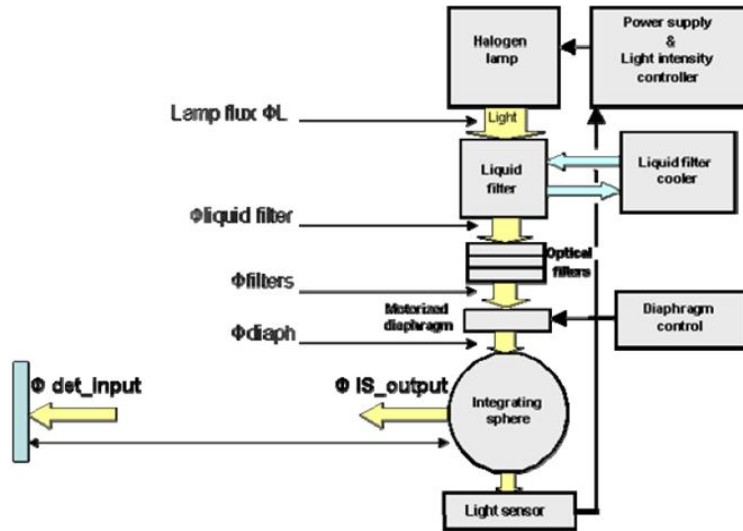


Fig. 2. Set-up for the radiometric tests performed at focal plane level

The following model gives the signal value provided by the focal plane (S_{FP}) electronics in the described laboratory set-up, at pixel p , when the focal plane center is receiving an irradiance $E(\lambda)$:

$$S_{FP}(E_{\lambda}, p) = K_{FP}(p) \cdot \int_0^{\infty} E(\lambda) \cdot R(\lambda) \cdot T_{FP}(p, \lambda) d\lambda + S_{FP}(0, p),$$

$$K_{FP}(p) = \frac{\tau \cdot \cos^4(\theta_p) \cdot (1 + K_{stray,FP}) \cdot (2^{nbit} - 1 - off) \cdot G}{10^4 \cdot V_{ADC}} \quad (1)$$

The parameters of (1) are described in table I. To be able to compare with the results of the radiometric campaign, the signal has to be expressed in terms of an average irradiance at the center of the field of view, \bar{E} :

$$\bar{E} = \int_{\lambda_1}^{\lambda_2} E(\lambda) \cdot T_{FP}^{ds,4^\circ}(p, \lambda) d\lambda \quad (2)$$

Where λ_1 and λ_2 are, respectively, the 1% cut-on and cut-off wavelengths of the focal plane windows for the spectral channel under analysis. The definition uses $T_{FP}^{ds,4^\circ}$, the focal plane spectral transmittance computed from the design (rather than the actual, measured) performance of the spectral band filter at an angle of incidence of 4° , to match the procedure followed during the radiometric campaign. It is worth to remark that, due to the used Korsch telescope concept, the light angle of incidence on the filters undergoes a significant variation across the field of view of the telescope, spanning the range of angles from 4° to 20° .

Table I. Parameters of the focal plane signal model

Symbol	Parameter	Units
S_{FP}	Digital signal at the electronics output, corresponding to pixel p at irradiance E_λ	[LSB]
$E(\lambda)$	Spectral irradiance at the center of the field of view	$[\text{mWm}^{-2}\mu\text{m}^{-1}]$
$R(\lambda)$	Detector spectral responsivity	$[\text{V}/\mu\text{J}/\text{cm}^{-2}]$
$T_{FP}(p,\lambda)$	Focal plane spectral transmittance corresponding to pixel p	$[\]$
$S_{FP}(0,p)$	Dark signal at pixel p	[LSB]
τ	Integration time	[ms]
θ_p	Light angle of incidence, on pixel p	$[\]$
$K_{\text{stray, FP}}$	Focal plane stray-light factor, only for contributors incrementing the signal level	$[\]$
n_{bit}	Pixel digitalization depth (12 bits)	[bits]
off	Digital video unit offset (31.5 LSB)	[LSB]
G	Electronic gain, proximity electronics	$[\]$
V_{ADC}	Video unit analog-to-digital converter maximum range	[V]

Dividing and multiplying the right-hand side of (1) by \bar{E} , we arrive to the following expression:

$$S_{FP}(\bar{E}, p) = \frac{K_{FP}(p) \cdot \int_0^\infty E(\lambda) \cdot R(\lambda) \cdot T_{FP}(p, \lambda) d\lambda}{\int_{\lambda_1}^{\lambda_2} E(\lambda) \cdot T_{FP}^{ds, A^\circ}(p, \lambda) d\lambda} \cdot \bar{E} + S_{FP}(0, p) = m_{FP}(p) \cdot \bar{E} + b_{FP}(p). \quad (3)$$

The slope of this line, m_{FP} , is invariant under multiplications of the center irradiance by a constant factor, and thus does not depend on the global illumination level. The slopes computed in this way have been matched to the ones measured on the radiometric campaigns at FP, as described in the next section.

ALIGNMENT OF THE FP SIGNAL MODEL TO RESULTS OF THE RADIOMETRIC CAMPAIGN

From the experimental radiometric data collected during the FP radiometric campaign, signal vs center irradiance plots can be generated for each pixel of the different spectral bands. An example of this type of graph is presented in fig. 3, for an arbitrary pixel in the MS-green spectral channel.

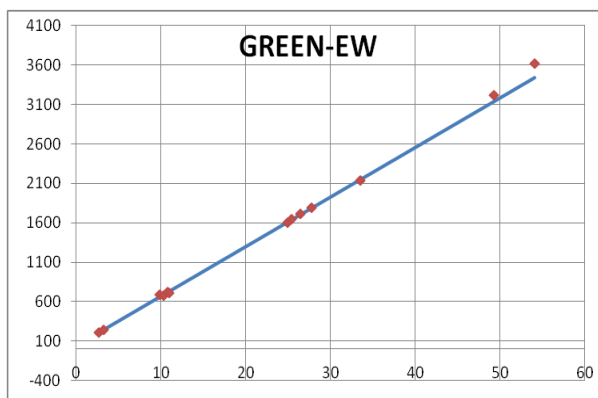


Fig. 3. Experimental digital output vs FP irradiance plot, for a pixel in the MS-green channel

The slopes computed from the model have been matched globally to the experimental ones, through multiplication by a constant factor (ie. not varying on a pixel by pixel basis) for each detector. This factor has then been included in the aligned radiometric model. To illustrate this point, in fig. 4 is included a graph with the values of the experimental slopes of all pixels in the PAN channel (depicted in blue) of the EQM focal plane, and the corresponding results of the model after alignment (in red). Each channel is constituted by the output of two adjacent detectors. Model slopes corresponding to the first detector (pixel numbers 1 to 6,000) have been multiplied by a factor of 1.11, to achieve an optimum alignment with the experimental data. For the second detector (pixel numbers 6,001 to 12,000), a factor of 1.10 has been considered. These alignment factors have been used subsequently in the flight radiometric model to derive flight signal predictions.

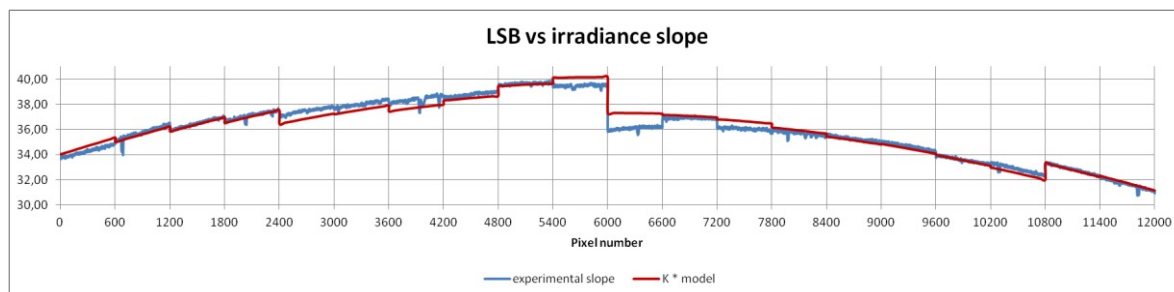


Fig. 4. Alignment of model (red line) and experimental slopes (blue), EQM-PAN channel

In table II are presented the alignment factors obtained by application of the described procedure to the four multi-spectral channels (blue, green, red and NIR) of the two focal plane flight models, FM- and FM+. The radiometric model considered here relied on the use of spectral responsivity measurements, only available in the project for MS channels. As could be seen, correlation between model predictions and measurements is excellent for all multi-spectral bands but MS-red. The higher discrepancy in this band is partly due to the presence of a spurious stray-light path, with an effect on this study.

Table II. Focal plane alignment coefficients, based on spectral responsivity measurements

Band	FM-		FM+	
	East	West	East	West
BLUE	1.02	0.95	1.02	0.99
GREEN	0.98	0.97	1.02	1.02
RED	1.14	1.05	1.09	1.05
NIR	1.00	0.98	0.99	1.00

Alternatively, in table III are presented alignment factors for a model based on the use of integrated responsivity measurements, rather than on spectrally resolved values. In our case, use of integrated responsivity measurements significantly increased the discrepancies between model predictions and measurements, compared to the use of spectral responsivities. In the project, models based on spectral responsivities have been used in all cases but for the PAN band, where only integrated responsivity values were available.

Table III. FP correlation coefficients, based on integrated responsivity measurements

Band	FM-		FM+	
	East	West	East	West
PAN	0.99	0.98	1.10	1.10
BLUE	1.20	1.15	1.23	1.20
GREEN	1.04	1.07	1.11	1.12
RED	1.15	1.11	1.15	1.11
NIR	1.09	1.09	1.11	1.11

EXPERIMENTAL DETERMINATION OF THE ELECTRONIC CHAIN AMPLIFICATION FACTOR

The described correlation procedure with radiometric results at focal plane level enables to identify deviations with respect to the nominal signal generation levels of the acquisition chain block dealing with the conversion from telescope image irradiance to digital signal output. As mentioned above, this could be thought of conceptually as a sequence of two steps, from irradiance values to a collection of generated photo-electrons, and from there to a digital signal.

It is possible to discriminate the effect of both steps using the concept of photon transfer curve. This curve [5-6] relates the observed noise variance to the mean signal level, and is thus dependent on the number of generated photo-electrons, which determines the magnitude of the photon shot noise term. Expressed in digital units, the photon transfer curve is given by the expression:

$$\sigma^2(E) = \sigma_{dark}^2 + K_Q \cdot (S(E) - S_{dark}), \quad (4)$$

with parameters described in table IV.

Table IV. Parameters of the photon transfer curve

Symbol	Parameter	Units
$\sigma^2(E)$	Noise variance (in LSB) at input irradiance E	[LSB ²]
σ^2_{dark}	Noise variance (in LSB) in darkness	[LSB ²]
K_Q	e- to LSB conversion factor	[LSB/e-]
$S(E)$	Signal at input irradiance E	[LSB]
S_{dark}	Signal in darkness	[LSB]

The parameter K_Q is given by the expression:

$$K_Q = \frac{(2^{\text{nbit}} - 1 - \text{off}) \cdot G \cdot CF}{10^6 \cdot V_{ADC}}, \quad (5)$$

where CF stands for the detector charge conversion factor, in units of $\mu\text{V}/\text{e-}$. Parameter K_Q value could be drawn from the radiometric model, or be estimated experimentally as the slope of lines fitted to $(S(E), \sigma^2(E))$ measurements, as in fig. 5. Comparison of model to experimental K_Q values could then be used to reveal deviations in the nominal electronic chain amplification factors. In the project, photon transfer curves have been used only tangentially for this purpose. Test performed have resulted in good agreement between experimental and model K_Q values for the PAN channel, with somewhat larger discrepancies found in multi-spectral channels.

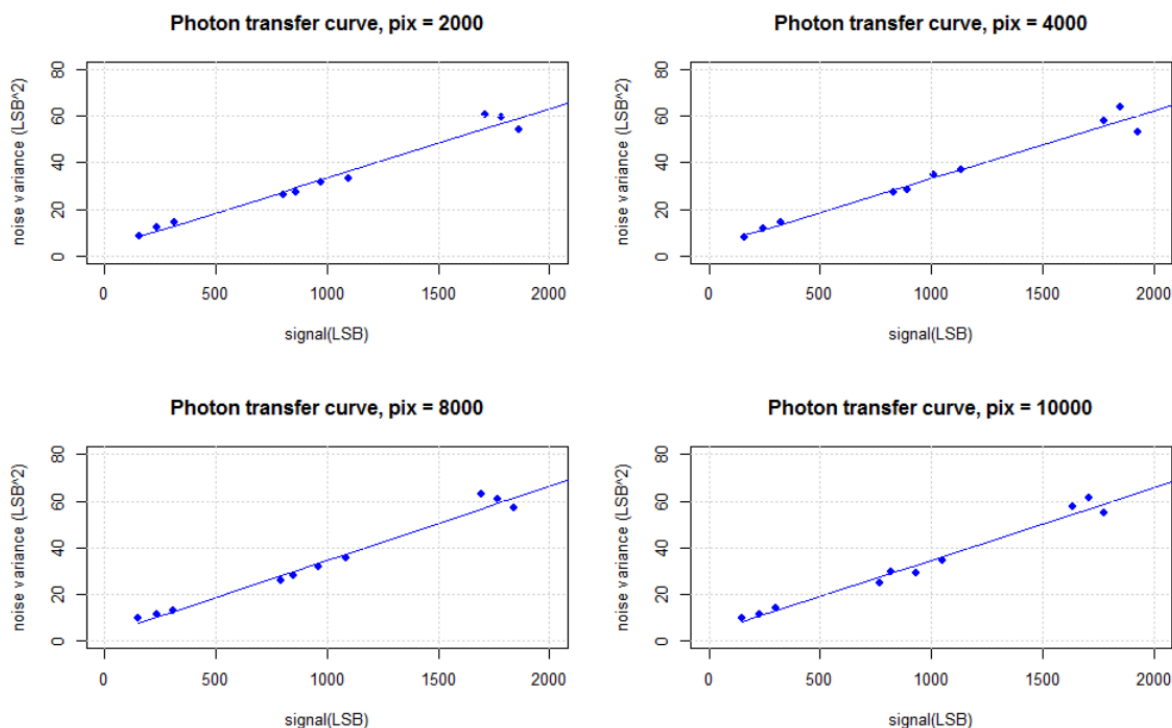


Fig. 5. Experimental photon transfer curves, PAN channel

CAMERA RADIOMETRIC SIGNAL MODEL

The following model gives the signal value provided by a camera (S_{CA}) in the laboratory set-up, at pixel p , when the telescope entrance pupil is receiving a radiance $L(\lambda)$:

$$S_{CA}(L_\lambda, p) = K_{CA}(p) \cdot \int_0^\infty L(\lambda) \cdot R(\lambda) \cdot T_{tel}(p, \lambda) \cdot T_{FP}(p, \lambda) d\lambda + S_{CA}(0, p),$$

$$K_{CA}(p) = \frac{\pi \cdot \tau \cdot I_{tel}(p) \cdot (1 + K_{stray, tel}) \cdot (1 + K_{stray, FP}) \cdot (2^{\text{nbit}} - 1 - \text{off}) \cdot (1 - \text{obs}(p)) \cdot G}{10^4 \cdot (1 + 4 F_\#^2) \cdot V_{ADC}} \quad (6)$$

The parameters of (6) not already present at focal plane level are described in table V. To compare with the results of the radiometric campaign, in this case the signal has to be expressed in terms of an average radiance at the entrance pupil, \bar{L} :

$$\bar{L} = \int_{\lambda_1}^{\lambda_2} L(\lambda) \cdot T_{tel}^{dsg}(p, \lambda) \cdot T_{FP}^{dsg, 4^\circ}(p, \lambda) d\lambda \quad (7)$$

Dividing and multiplying the right-hand side of (6) by \bar{L} , we arrive to the following expression:

$$S_{PP}(\bar{L}, p) = \frac{K_{CA}(p) \cdot \int_0^\infty L(\lambda) \cdot R(\lambda) \cdot T_{tel}(\lambda) \cdot T_{FP}(p, \lambda) d\lambda}{\int_{\lambda_1}^{\lambda_2} L(\lambda) \cdot T_{tel}^{dsg}(\lambda) \cdot T_{FP}^{dsg, 4^\circ}(\lambda) d\lambda} \cdot \bar{L} + S_{CA}(0, p) = m_{CA}(p) \cdot \bar{L} + b_{CA}(p). \quad (8)$$

Table V. Parameters exclusive to the camera signal model

Symbol	Parameter	Units
$S_{CA}(L_\lambda, p)$	Digital signal at camera output, corresponding to pixel p at radiance L_λ	[LSB]
$L(\lambda)$	Input spectral radiance	[mWm ⁻² sr ⁻¹ μm ⁻¹]
$T_{tel}(\lambda)$	Telescope spectral transmittance	[]
$I_{tel}(p)$	Relative nominal irradiance distribution at pixel p	[]
$K_{stray, tel}$	Telescope stray-light factor, for contributors incrementing the signal level	[]
obs	Obscuration ratio at the telescope entrance pupil, due to M2, spiders, etc	[]
$F_\#$	Telescope f-number	[]

The ratio of slopes at focal plane and complete camera levels is proportional to the following expression, for pixel p:

$$\frac{m_{CA}(p)}{m_{FP}(p)} \propto \frac{I_{tel}(p) \cdot (1 + K_{stray, tel}) \cdot (1 - obs(p)) \cdot \overline{T_{tel}}}{(1 + 4 F_\#^2) \cdot \cos^4(\theta_p)}, \quad (9)$$

where the proportionality factor involves only focal plane and telescope as-designed spectral transmittances, directly connected to the definitions used for average irradiance and radiance. Hence, this factor will not change as long as the used definitions for these parameters remain in place. The appearing $\overline{T_{tel}}$ factor is a spectrally averaged telescope transmittance, with weights given by the multiplication of the spectral radiance and the transmittance of the focal plane optics. This value is not dependent on changes of the focal plane transmittance peak value, as long as the designed transmittance band shape is not significantly perturbed. The rest of intervening parameters pertain only to the telescope.

As a consequence, a deviation of the ratio of both slopes with respect to its design value is directly linked, under realistic assumptions, to a modification in one of the telescope parameters appearing in (9). This has been used to derive alignment factors for the telescope contribution, as described in the following section.

ALIGNMENT OF THE RATIO OF SLOPES MODEL TO RESULTS OF THE RADIOMETRIC CAMPAIGN

Radiometric tests at camera level have been performed by placing a large aperture integrating sphere in front of the telescope entrance pupil. In an analogous way as for the radiometric campaigns performed at focal plane level, signal vs mean radiance plots have been generated for each pixel of the different spectral bands. From these slopes, together with the corresponding ones at focal plane level, the slope ratio presented in (9) has been determined experimentally.

Slopes computed from the model have been matched globally to the experimental ones, multiplying model slopes by a constant factor per detector. As for the focal plane assembly, this factor has then been included in the aligned radiometric model. In fig. 6 is included a graph with the values of the experimental ratio of slopes for all pixels in the PAN channel (depicted in blue) of the EQM focal plane, and the corresponding results of the model after alignment (in red).

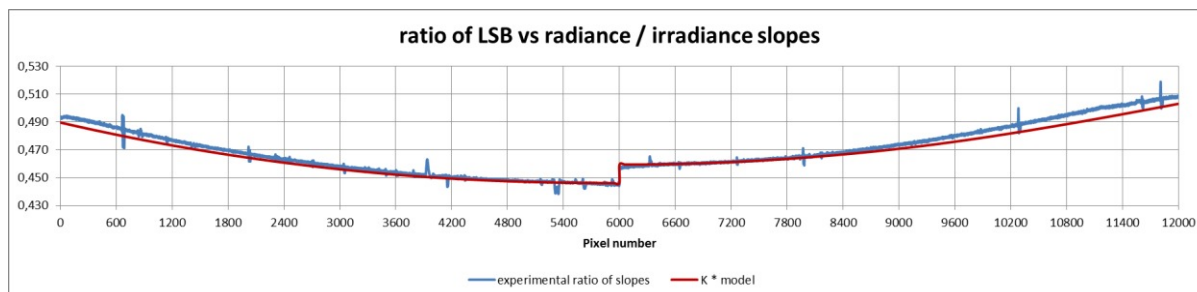


Fig. 6. Alignment of model (red line) and experimental ratio of slopes (blue), EQM-PAN channel

In table VI are presented the telescope alignment factors obtained by application of the described procedure to the PAN and MS channels of the EQM model, the only model for which radiometric measurements at complete camera level are currently available. As shown, this telescope alignment factor is independent of the focal plane model used in the measurements, and has therefore been used without modification in the aligned flight signal model.

A good agreement between model predictions and measurements has been obtained for the telescope contribution. The obtained average alignment factor is around a 4%, in the order of magnitude of the accuracy of the spectro-radiometer used to calibrate the radiometer set-ups (3.5%).

Table VI. FP correlation coefficients, telescope contribution

Band	
PAN	1.04
BLUE	1.07
GREEN	1.03
RED	1.00
NIR	1.07

CONCLUSIONS

The methodology and results of the correlation performed in the framework of SEOSAT project between the theoretical signal model and the results of the radiometric campaigns has been presented in detail. The work is based on the use of the slopes of the signal transfer functions at both focal plane and complete camera levels. The method presented provides a method to derive camera correction factors from telescope and focal plane contributors and constitutes a system-level approach to determine the contribution to the output signal of different blocks of the acquisition chain, based exclusively on results generally available from different radiometric campaigns.

REFERENCES

- [1] A. Marini, F.J. Reina Barragan, G. Crippa, B. Harnisch *et al.*, “SEOSAT/INGENIO - A SPANISH HIGH-SPATIAL-RESOLUTION OPTICAL MISSION”, *International Conference on Space Optics(ICSO)*, CNES-ESA, October 2014.
- [2] C. Miravet, D. Zorita, J.I. Bueno, L. Pascual *et al.* “Development status of the telescope for the Ingenio/SEOSAT mission primary payload”, *Proc. SPIE 8167, Optical Design and Engineering IV*, September 2011.
- [3] L. Pascual, J.I. Bueno, D. Zorita, C. Miravet *et al.*, “Detailed Optical Design of SEOSAT/Ingenio Spanish High Resolution Imaging Instrument”, *International Conference on Space Optics(ICSO)*, CNES-ESA, October 2012.
- [4] D. Zorita, C. Miravet, J.I. Bueno, “Challenges and developed solutions for the principal payload of the SEOSAT/Ingenio mission”, *RAQRS III, Recent Advances in Quantitative Remote Sensing*, September 2010.
- [5] J. R. Janesick, *Scientific Charge-Coupled Devices*, SPIE Press Monograph Vol. PM83, 2001.
- [6] J. R. Janesick, *Photon transfer*, SPIE Press Monograph Vol. PM83, 2001.